Biochemistry

Article

pubs.acs.org/biochemistry

Mobility and Core-Protein Binding Patterns of Disordered C-Terminal Tails in β-Tubulin Isotypes

Yoann Laurin,[†] Joel Eyer,[‡] Charles H. Robert,[†] Chantal Prevost,[†] and Sophie Sacquin-Mora*[,†]

[†]Laboratoire de Biochimie Théorique, UPR 9080 CNRS, Institut de Biologie Physico-Chimique, 13 rue Pierre et Marie Curie, 75005 Paris, France

[‡]Laboratoire de Neurobiologie & Transgenèse, UPRES EA 3143, INSERM, Centre Hospitalier Universitaire, Angers, France

Supporting Information

ABSTRACT: Although they play a significant part in the regulation of microtubule structure, dynamics, and function, the disordered C-terminal tails of tubulin remain invisible to experimental structural methods and do not appear in the crystallographic structures that are currently available in the Protein Data Bank. Interestingly, these tails concentrate most of the sequence variability between tubulin isotypes and are the sites of the principal post-translational modifications undergone by this protein. Using homology modeling, we developed two complete models for the human αI/βI- and αI/βIII-tubulin isotypes that include their C-terminal tails. We then investigated the conformational variability of the two β-tails using long time-scale classical molecular dynamics simulations that revealed similar features, notably the unexpected presence of common anchoring regions on the surface of the tuulin dimer, but also distinctive mobility or interaction patterns, some of which could be related to the tail lengths and charge distributions. We also observed in our simulations that the C-terminal tail from the βI isotype, but not the βIII isotype, formed contacts in the putative binding site of a recently discovered peptide that disrupts microtubule formation in glioma cells. Hindering the binding site in the βI isotype would be consistent with this peptide's preferential disruption of microtubule formation in glioma, whose cells overexpress βIII, compared to normal glial cells. While these observations need to be confirmed with more intensive sampling, our study opens new perspectives for the development of isotype-specific chemotherapy drugs.

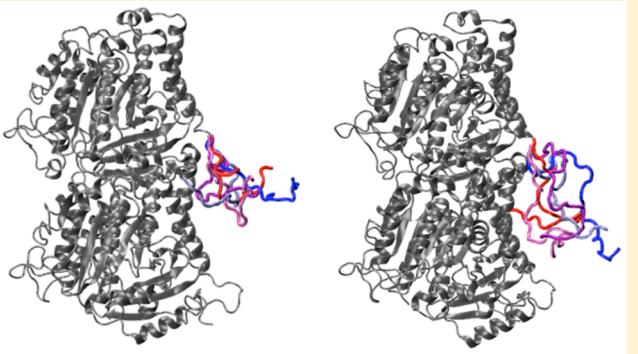

Microtubules (MTs) are rigid tubular fibers composed of α/β-tubulin heterodimers and are key components of the cytoskeleton, controlling essential cellular functions such as mitosis, cell signaling, and intracellular transport.[1] In many organisms, both α- and β-tubulins are encoded by multigene families, comprising, for instance, six and seven isotypes, respectively, in the human genome.[2] While specialized cells may express a single isotype, most tissues will express several, and as a result, microtubules are usually made of a mixture of isotypes with their composition varying by cell type.[3] Tubulin isotype βIII has been by far the most extensively studied in human cancer. Its expression in normal cells and tissues is usually neuronally associated, but it is also widely observed in numerous human malignancies[4,5] and has been identified as a strong indicator of poor clinical outcomes.[6]

On the MT outer surface, the well-defined tubulin globular domain is decorated by a highly charged carboxy-terminal tail (CTT) thought to play a critical role in regulating MT assembly.[7−14] Interestingly, CTTs of α- and β-tubulin are the main sites of sequence variation among isotypes. For example, βI, the most frequently expressed isotype, and βIII isotypes differ by only 13 amino acids within their 1−429 fragment, while their CTTs are completely different.[5] CTTs are also the site of the majority of post-translational modifications (such as tyrosination, glutamylation, or phosphorylation[15,16]). Despite its important role in proper MT assembly, little is known about the CTT conformation and its impact on tubulin's interaction with other proteins. Early experimental studies using nuclear magnetic resonance (NMR) and circular dichroism have shown that CTTs are disordered segments,[17,18] and as a consequence, they do not appear in the tubulin crystal structures currently available in the Protein Data Bank (PDB).

Because of the critical role they play in mitosis, MTs are important cancer drug targets. Antimitotic compounds interfere with the polymerization or depolymerization of α,β-tubulin dimers into MTs, thus inhibiting cancer cell division and proliferation.[19,20] Widely used antitumor drugs include taxanes, vinca alkaloids or colchicin, which interact with tubulin via three distinct and well-documented binding sites.[19−21] Remarkably, none of these sites lie near the tubulin CTTs, and therefore, most molecular modeling studies of tubulin−ligand interactions did not include this disordered segment in

Received: September 28, 2016
Revised: March 10, 2017
Published: March 14, 2017

DOI: 10.1021/acs.biochem.6b00988
Biochemistry XXXX, XXX, XXX−XXX

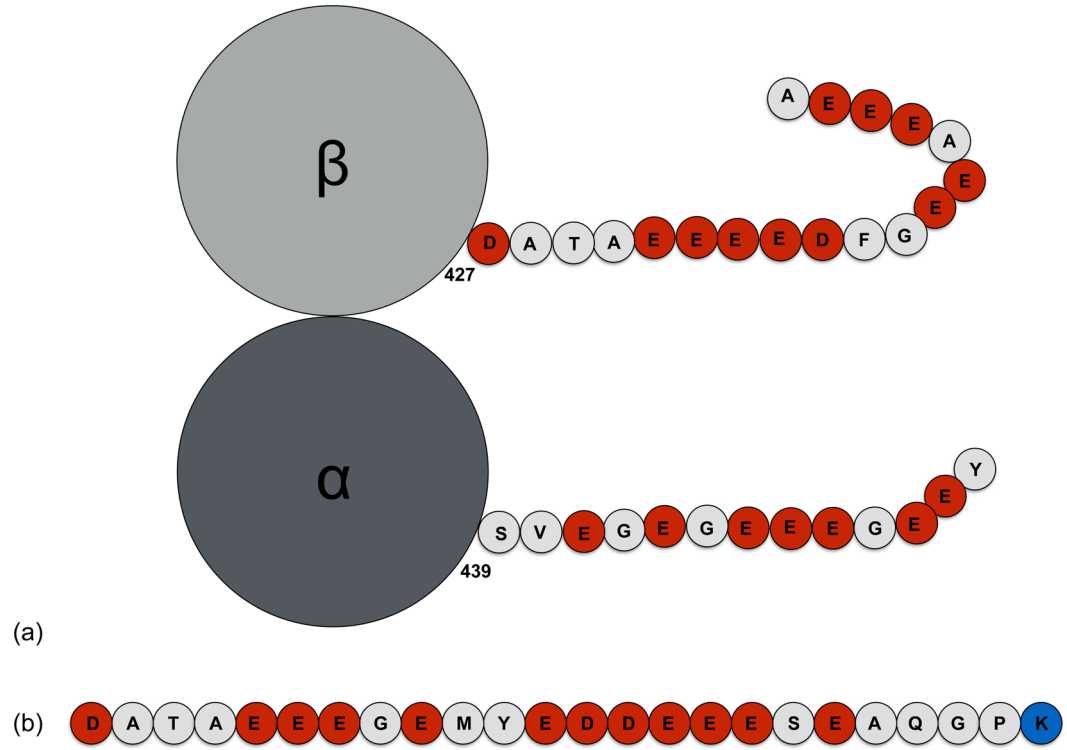

Figure 1. (a) Schematic representation of the αI/βI-tubulin heterodimer showing the amino acid sequences for the C-terminal tails. (b) Amino acid sequence for the C-terminal tail of the βIII isotype. In both panels, negatively charged residues are colored red and positively charged residues blue.

their representation.[21−28] More generally, few theoretical studies of tubulin take into account the CTTs, although, in a seminal work, Luchko et al. investigated the conformational variability of the isolated β-CTTs for nine isotypes using replica exchange molecular dynamics simulations, but without taking into account the main tubulin globular domain.[29] Subsequently, Freedman et al. used molecular dynamics to predict the interaction of the C-terminal tails with the tubulin heterodimer in the case of the human αIV-βI isotype.[30] Two additional studies explicitly model the CTTs while investigating the interaction of tubulin with proteins like γ-synuclein[31] or kinesin,[32] which bind the tubulin surface in the vicinity of the CTTs.

The NFL-TBS.40−63 peptide is a recently discovered tubulin binding agent derived from the light neurofilament protein, which has demonstrated a high capacity for the inhibition of microtubule formation in an *in vitro* polymerization assay.[33] Further studies of this peptide have shown that *in vitro* it is more efficiently internalized by glioma cells than by normal cells, this difference not being species-specific.[34] Moreover, once internalized by glioma cells, the peptide strongly affected their microtubule network, attenuated proliferation, and led to apoptosis. These *in vitro* properties of the NFL-TBS.40−63 peptide were also observed *in vivo*, when the peptide was injected into the brains of glioma-bearing rats, and make this peptide a promising candidate for malignant glioma treatment. Our own previous modeling study of the interaction modes of the NFL-TBS.40−63 peptide on the tubulin surface[35] showed that, while lacking a stable structure, the peptide may bind to a unique specific site located near the β-tubulin CTT. This suggests that the NFL-TBS.40−63 peptide binding to this site might hinder MT formation and its dynamic regulation in the cell by modifying the β-C-terminal tail mobility, thus preventing important intra- and interdimer contacts within MTs, and interfering with MT-associated proteins that usually bind on the MT's outer side. As a consequence, the proper modeling of the CTT dynamics appears to be an essential issue, if we want to understand correctly on a molecular level the interaction between the NFL-TBS.40−63 peptide and tubulin.

In this perspective, using homology modeling, we developed two complete models for the human αI/βI- and αI/βIII-tubulin isotypes that include their C-terminal tails. We then investigated the mobilities of these two β-CTTs using classical molecular dynamics (MD) simulations and showed how each appears to present specificities in its interaction pattern with the tubulin surface that may be related to its length and charge distribution. As mentioned previously, tubulin isotype βIII is overexpressed in cancer cells, and this overexpression is associated with resistance to antimitotic drugs such as taxanes.[4,36] Therefore, our work helps pave the way for a better understanding of the molecular origins of this resistance and opens new perspectives for the development of isotype-specific chemotherapy drugs.

MATERIALS AND METHODS

Complete Models for the Human Tubulin Isotypes. We used homology modeling to build the human αI/βI- and αI/βIII-tubulin isotypes. Each heterodimer is based on the same template, i.e., a double tubulin heterodimer bound with stathmin (PDB entry 1SA0), which was chosen for its high degree of similarity with the target sequences and which is the most complete of all available crystal structures. The 1SA0 structure is already present in the template database of Modeller version 9.14 that we used, which also includes the 1TUB structure and domains of FtsZ, a prokaryotic homologue of tubulin. The Modeller process is based on a classic comparative modeling method consisting of four sequential

DOI: 10.1021/acs.biochem.6b00988
Biochemistry XXXX, XXX, XXX−XXX

steps: template selection, template−target alignment, model building, and a final model evaluation.[37,38] The target sequences for human tubulin were retrieved from the UniProtKB Web site[39] as accession numbers Q71U36, P07437, and Q13509 for the αI-, βI-, and βIII-subunits, respectively. Because of the high degree of similarity between the target sequences and the structural templates [>75% sequence identity (see Table SI-1)], there was no need for a manual rearrangement of the alignments. To model the tubulin CTTs, which are not present in the template structures, Modeller performs an ab initio conformational search. For each β isotype, the five CTT structures with the lowest Modeller score, based on energy scores [DOPE and MolPDF (see Table SI-2)], were selected. Note that for each tubulin isoform, the selected CTT structures present very similar energy scores with around 1 and 10% variations for the DOPE and MolPDF scores, respectively.

The CTT for the αI-subunit starts with residue αSer439 and contains 13 amino acids; in the case of the βI- and βIII-subunits, the CTT starts with residue βAsp427 and contains 18 and 24 amino acids, respectively (see Figure 1). The conventional protonation states at pH 7.0 were used for all residues; as a consequence, the β-CTTs in both isotypes bear an important negative charge (−11*e*), because of their high number of glutamate and aspartate residues (see Table 1). Note that the βIII-CTT ends with a lysine residue bearing a positive charge. Subunits, modeled separately, were assembled to form straight αI/βI and αI/βIII heterodimers using a spatial alignment on the highest-resolution structure available for this conformation (PDB entry 1JFF, resolution of 3.5 Å). Finally, before performing MD simulations, we used SCWRL4[40] on the tubulin heterodimers to optimize the side-chain conformations.

Table 1. Clustal Multiple-Sequence Alignment for the β-CTTs in Human Tubulin

Isotype	Sequence	Length
I (P07437)	DATAEEEE--DFGEEAEEEA	18
III (Q13509)	DATAEEEG--EMYEDDEEESEAQGPK	24

Molecular Dynamics Simulations. For both αI/βI and αI/βIII heterodimers, we then performed MD simulations on each of the five models that were produced with different conformations of the β-CTTs. We used Gromacs,[41] version 5.0.4, with the OPLS-AA force field[42] with periodic boundary conditions. The first step of the simulation procedure is an *in vacuo* minimization of the structure with the steepest descent algorithm during 1000 steps without any constraints. We added a triclinic water box of 2 nm around the tubulin, filled with a TIP3P molecule type,[43] and the system was neutralized with the addition of ions randomly placed in the box while maintaining the NaCl concentration at 150 mM. The total system contains around 13700 atoms for the tubulin heterodimer, 136000 water molecules, and 320 ions (with approximatively 180 Na^+ and 140 Cl^- ions, because of the highly negatively charged CTTs). A second minimization step was performed with the same set of parameters as before during 5000 steps to prevent possible water clashes with the tubulin. Molecular dynamics were performed using an integration time step of 2 fs. Initial heating and pre-equilibration were performed by assigning random velocities from the Maxwell−Boltzmann distribution followed by 100 ps of dynamics under *NVT* conditions and then 100 ps under *NPT* conditions. During this process and for all subsequent dynamics, the temperature was fixed at 300 K using the velocity rescale method.[44] All bonds were constrained with the LINCS algorithm,[45] and electrostatic interactions were computed using the particle mesh Ewald method.[46] For pressure coupling during the *NPT* equilibration, we used the Parinello−Rahman method[47] at a value of 1 atm. Production phases were finally done using the same set of parameters and algorithms during 100 ns. Trajectories were saved every 10 ps.

Trajectory Analysis. Gromacs utilities were used for basic observations along with VMD[48] for visual inspection. More elaborate analyses used homemade scripts or programs. As the root-mean-square deviation (RMSD) is not sufficient for investigating the flexibility of the β-terminal tails during the MD simulations, we performed additional analysis of the CTT position with regard to the main tubulin heterodimer axis (axis *z* in Figure 2), radius of gyration, and pattern of contacts with the main tubulin body.

RESULTS

Electrostatic Properties of the Tubulin Core. As shown in Figure 3, the two αI/βI and αI/βIII isotypes present similar

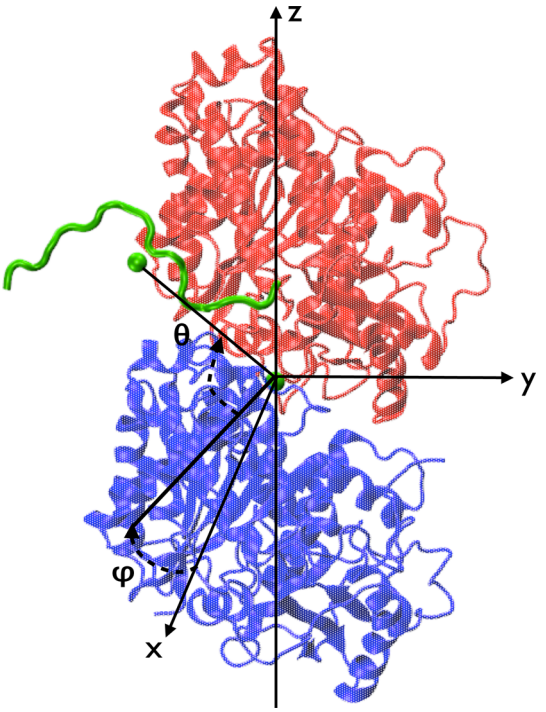

Figure 2. Cartoon representation of the tubulin heterodimer with the α-subunit colored blue, the β-subunit colored red, and the β-CTT colored green. The centers of mass for the tubulin heterodimer and the β-CTT are shown as green spheres. The black axes show the orthonormal reference system used for defining the position of the β-CTT's center of mass via angles φ and θ. The direction of the *z* axis is defined by the centers of mass of the α- and β-subunits (positive in the β-subunit direction), while the *x* axis is defined perpendicular to this line, passing through the CA atom of the residue at the base of the C-terminal tail and thus also setting the origin of the coordinate system. The φ angle defines the lateral displacement of the β-CTT's center of mass within the *x*−*y* plane and with regard to the *x* axis, while the θ angle defines its vertical displacement with regard to the *x* axis. This figure was prepared using visual molecular dynamics.[48]

DOI: 10.1021/acs.biochem.6b00988
Biochemistry XXXX, XXX, XXX−XXX

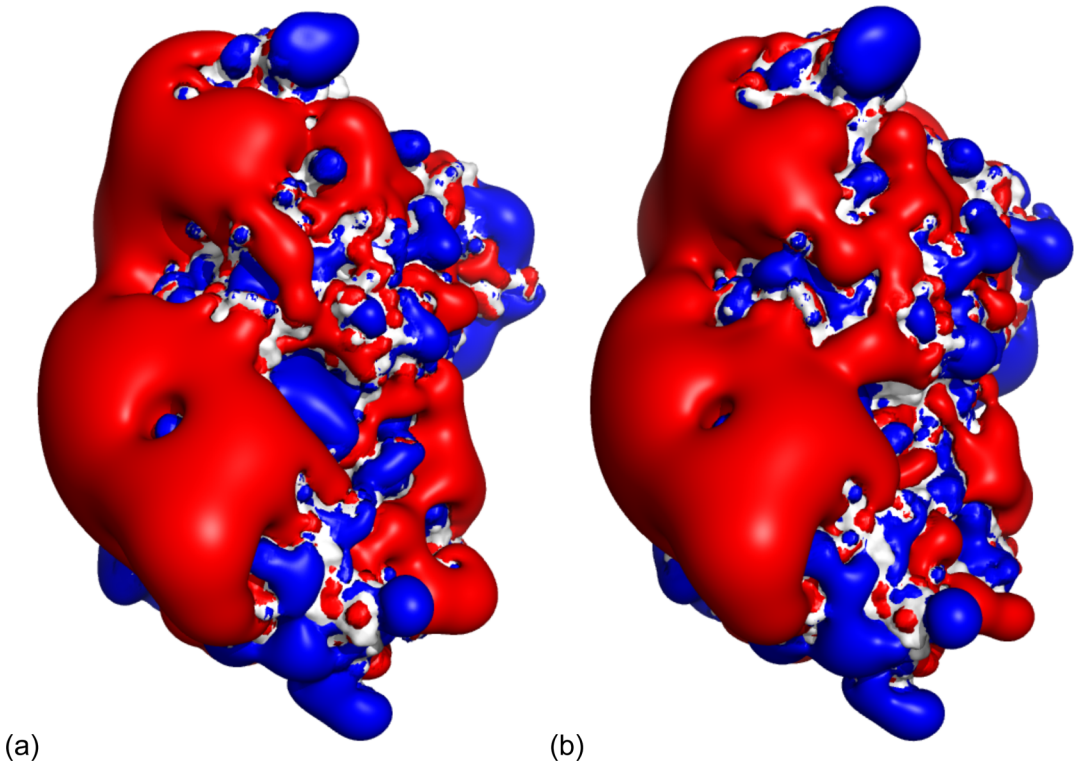

Figure 3. Surface electrostatic potential (±1 kT) of the tubulin body (without the CTTs) resulting from APBS calculations. Positive potentials are colored blue and negative potentials red: (a) αI/βI isotype and (b) αI/βIII isotype. The tubulin heterodimer has the same orientation as in Figure 1. This figure and Figures SI-6 and SI-7 were prepared using PyMol.[64]

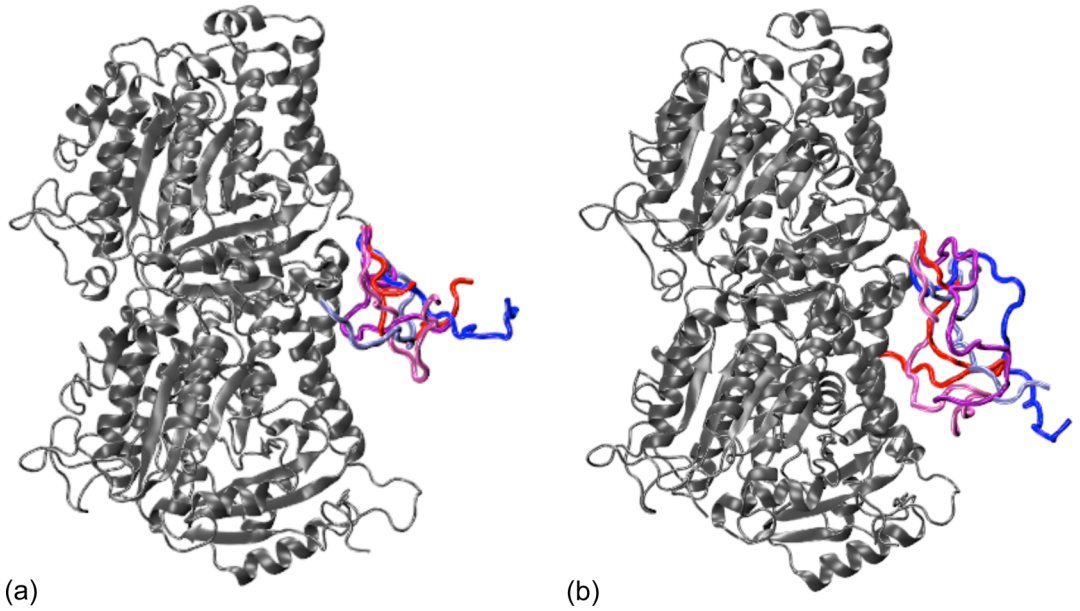

Figure 4. Cartoon representation showing the tubulin heterodimer (gray) with the starting structures of the β-CTTs for the five MD trajectories colored red, magenta, purple, dark blue, and light blue. The tubulin orientation has been rotated by 90° around the vertical axis with regard to Figure 1: (a) αI/βI isotype and (b) αI/βIII isotype. The color code for the five trajectories of each isotype is the same in Figures 5, 7, 8, and 10. This figure was prepared using visual molecular dynamics.[48]

surface electrostatic potentials, which were calculated using the APBS Web server,[49] with both heterodimers presenting a large electronegative groove on their α-subunit and no noticeable variations between the βI- and βIII-subunits.

β-C-Terminal Tail Structure and Flexibility. Figure 4 shows the starting structures of the β-CTTs for the αI/βI and αI/βIII heterodimers. For the five trajectories performed for each isotype, the CTTs are initially unfolded, mostly solvated, and directed toward the tubulin α-subunit (bottom part of Figure 4). From the RMSD plots shown in Figure 5, we can see that the structure of the heterodimer core (which does not include the CTTs) remains very stable during the simulations,

DOI: 10.1021/acs.biochem.6b00988
Biochemistry XXXX, XXX, XXX−XXX

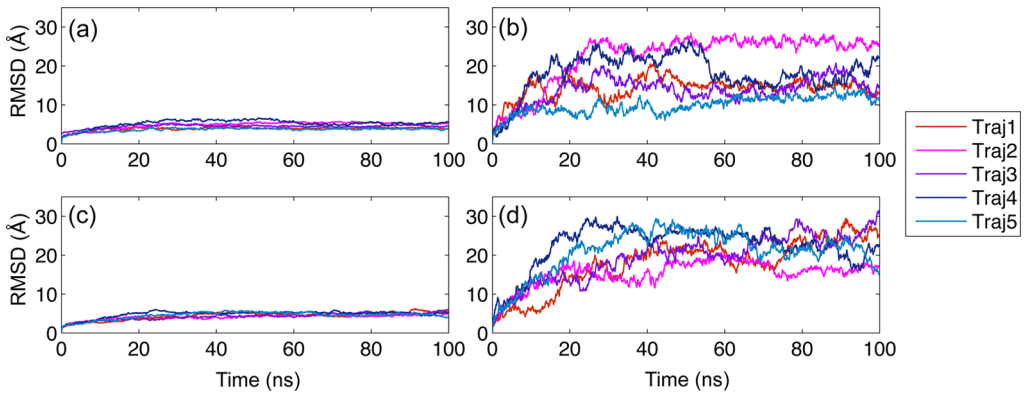

Figure 5. RMSDs during the five MD trajectories for the tubulin heterodimer core and β-CTT in each isotype. αI/βI isotype: (a) core and (b) β-CTT. αI/βIII isotype: (c) core and (d) β-CTT.

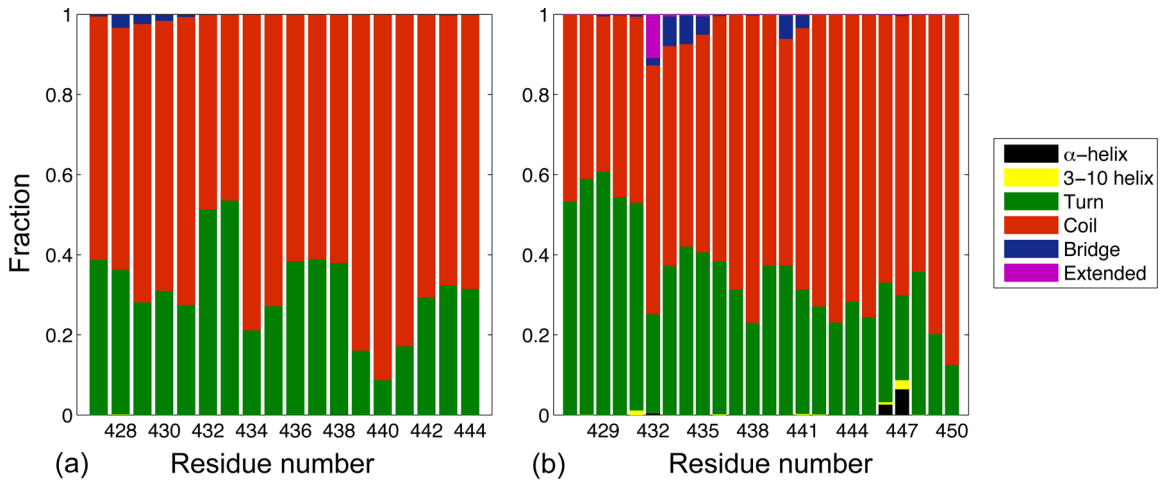

Figure 6. Time average of each secondary structure for each β-CTT. The total fractional secondary structure content was determined as an average over the five 100 ns MD simulations. The fractional time averages of each secondary structure are stacked to sum to one. The color code is based on Figure 3 of ref 29 to allow a direct visual comparison: (a) αI/βI isotype and (b) αI/βIII isotype.

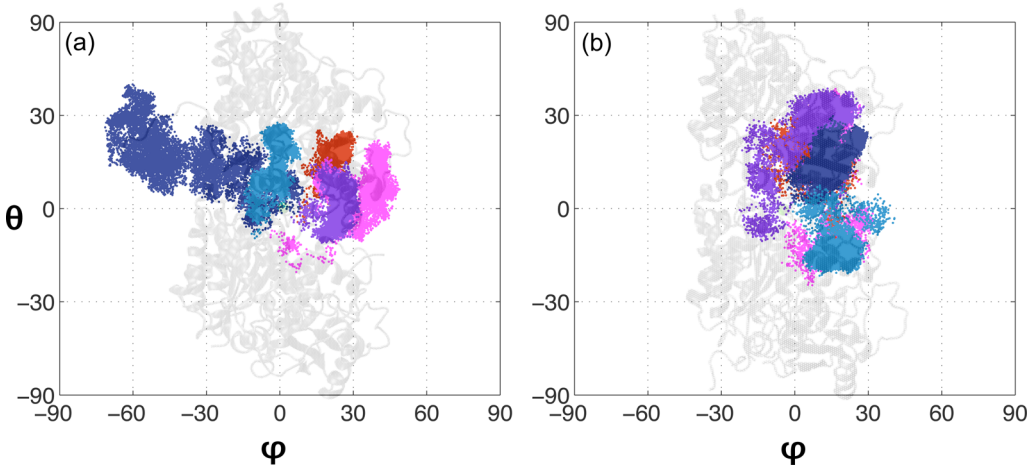

Figure 7. Mobility of the β-CTT center of mass during the five MD trajectories for each isotype. The tubulin heterodimer is shown as a transparent cartoon in the background as a visual guide: (a) αI/βI isotype and (b) αI/βIII isotype.

while the highly flexible β-tails display a large RMSD from the initial conformation with time. Root-mean-square fluctuations on the β-CTTs α-carbons lead to similar results (see Figure SI-1), showing large structural fluctuations. Figure 6 shows the time average of each type of secondary structure for the β-CTT in each isotype as calculated over the five 100 ns MD simulations by STRIDE.[50] In both cases, the tails remain unstructured during most of the trajectories, with their residues adopting essentially turn and coil conformations.

Mobility of the β-C-Terminal Tails. The mobility of the β-CTTs was monitored along the five MD trajectories by looking at the position of their center of mass, using the φ and

DOI: 10.1021/acs.biochem.6b00988
Biochemistry XXXX, XXX, XXX−XXX

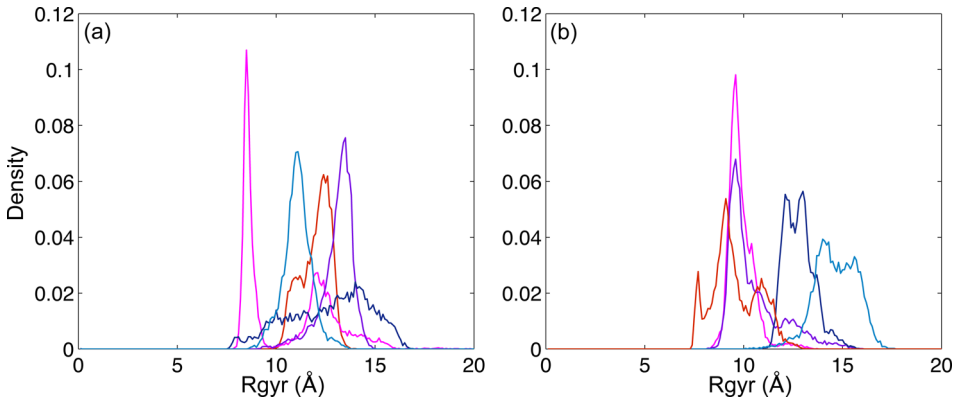

Figure 8. Density plot for the radius of gyration of the β-CTTs during the five MD trajectories for each isotype: (a) αI/βI isotype and (b) αI/βIII isotype.

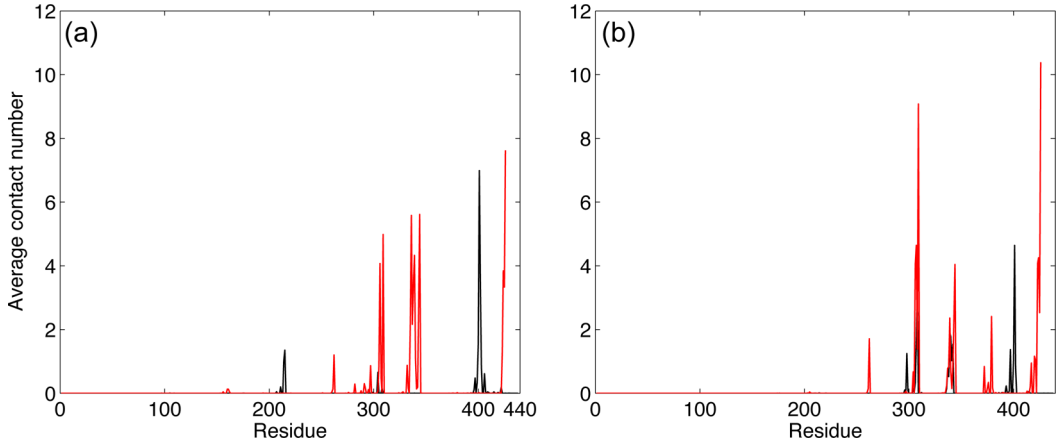

Figure 9. Average contact number between the tubulin core residues and the β-CTT over the five MD simulations. The black line shows contacts between the α-subunit and the β-CTT. The red line shows contacts between the β-subunit and the β-CTT: (a) αI/βI isotype and (b) αI/βIII isotype.

θ angles defined in Figure 2. The resulting scatter plots are shown in Figure 7. For the αI/βI isotype, after an initial vertical movement toward the β-subunit (which corresponds to positive θ values in Figure 7), the β-CTT's center of mass explores a restricted space around the interface between the α- and β-subunits, with the exception of trajectory 4 (shown with dark blue points in Figure 7a), in which the β-CTT displays a significant shift toward the left side of the tubulin heretodimer. The distributions of the β-CTT's radius of gyration along the trajectories are shown in Figure 8a for the αI/βI isotype. In trajectories 1−3 and 5, the limited displacement of the β-CTT over the tubulin surface leads to one or two well-defined density peaks for the radius of gyration between 8.5 and 14 Å. In the case of trajectory 4 (dark blue line in Figure 8a), the exploration of a wider area of the tubulin surface by the β-CTT results in a broader distribution for its radius of gyration, which can reach 16 Å when the tail adopts an extended conformation.

In the case of the αI/βIII isotype, the longer β-CTT undergoes vertical displacements that tend to be larger than those of the βI-CTT (see the next section) during the five MD simulations, with more limited lateral moves than for the αI/βI isotype. During trajectory 5 in particular (shown by light blue points in Figure 7b), the β-CTT explores the surface of the α-subunit (which corresponds to negative θ values in Figure 7) behind the large electronegative groove that is visible in Figure 3. While the β-CTTs in both isotypes bear a high negative charge ($-11e$), in the case of the βIII isotype, the CTT is terminated by a positively charged lysine residue that facilitates the contact between the tail and the α-subunit. The distribution peaks for the radius of gyration (shown in Figure 8b) are slightly shifted toward larger values (from 9 to 15.5 Å) compared with those of the αI/βI isotype, which is consistent with the longer length (six additional residues) of the CTT in the βIII isotype. The radius of gyration distribution for trajectory 5 (light blue line in Figure 8b) displays the largest values, because the terminal tail adopts an extended conformation to explore the surface of the α-subunit.

Tail−Body Interactions. We investigated contacts formed by the β-CTT and the tubulin core residues during the simulations, identifying a contact between two residues when any of their heavy atoms are within 4 Å of each other.[51] Figure 9 shows the tubulin core residues that are in contact with the β-CTT during the MD simulations. Analysis of the spatial distribution of core residues contacted by the β-CTT suggests that they differ for the βI and βIII isotypes. Via comparison of time-averaged values of the θ angle of the contacted core residues for each MD run, which corresponds to measuring their vertical dispersion (Figure 2), the contacts made by the βI-tails were more clustered at values near the α/β-subunit interface than those of the βIII-tails (93% confidence in rejection of the null hypothesis by the nonparametric Mann−Whitney U test).

DOI: 10.1021/acs.biochem.6b00988
Biochemistry XXXX, XXX, XXX−XXX

The βIII-CTT also formed more contacts with the α-subunit than its βI counterpart, as can be seen from the black lines in panels a and b of Figure 9, especially in trajectory 5. Figures SI-2 and SI-3 reveal that for both isotypes, most tail−body interactions tended to occur via a limited number of residues from the tubulin surface, namely, Lys401 for the α-subunit and Arg306, Arg309, Lys336, Ser339, and Trp344 for the β-subunit.

Looking in more detail at the trajectories produced by the MD simulations for the two tubulin isotypes (an archive containing animated gifs of all the trajectories is available as Supporting Information), we notice that in almost all cases, at some point during the simulation, the β-CTT binds to a residue from the tubulin core, located on the α- or β-subunit, that we call an anchor residue. Once this contact is formed, it is conserved for the rest of the simulation, thus restricting the global mobility of the β-CTT. Figure 10 displays snapshots taken from our 10 MD simulations with characteristic structures of the β-CTT (colored following the same code as in Figure 4) and the anchor residue (chosen from Figures SI-2 and SI-3 as the tubulin core residue forming the largest number of contacts with the β-CTT during the simulation) for each trajectory colored green. An exception to this behavior appears during trajectory 4 for the αI/βI isotype, in which the β-CTT presents an enhanced lateral mobility (as shown by the dark blue points in Figure 7a). In this case, the tail residues transiently bound the surface of the heterodimer's βI-subunit (see Figure 10d) before ending in a fully extended and solvated state. While most anchor residues are located in the vicinity of the α/β-subunit interface, in trajectory number 5 of the αI/βIII isotype the β-CTT displays an extended conformation, with its extremity bound to the lowest part of the α-subunit (see the snapshot in Figure 10j). We also investigated which specific residues from the β-CTT bound the anchor residues during the simulation time for each trajectory (see Figures SI-4 and SI-5). Interestingly, a single anchor residue may interact with different parts of the β-CTT in different trajectories, or at different instants from the same trajectory. αLys401, for example, essentially binds the base of the β-CTT [βAsp427, βAla428, and βThr429 (see Figure SI-4a)] during trajectory 1 for the αI/βI isotype, while in trajectory 5, it forms contacts with the end of the β-CTT [βGlu441 and βGlu442 (see Figure SI-4e)]. In trajectory 3 for this same isotype, we can see how the terminal tail shifts on the surface of the tubulin via the changes over time for the contact patterns of βLys366 and βSer339 (see Figure SI-4c). Finally, for the αI/βIII isotype, it is interesting to watch how βArg306's contacts with the β-CTT base are eventually broken and replaced by contacts with the tails' end in trajectory 1 (see Figure SI-5a).

On the β-CTT side, the residues forming contacts with the tubulin core varied widely from one trajectory to the other, as shown in Figure SI-6, with the exception of the first two residues located at the base of the tail, which always remained close to the core surface. Depending on the trajectory, tail residues were found in either a mostly bound or a mostly solvated state, and no two trajectories present the same contact pattern in the β-CTT tail residues. The only noticeable exceptions were residues βAsp435 and βPhe436 from the αI/βI isotype, which were bound to the tubulin core surface most of the time for all five MD simulations (see Figure SI-6a).

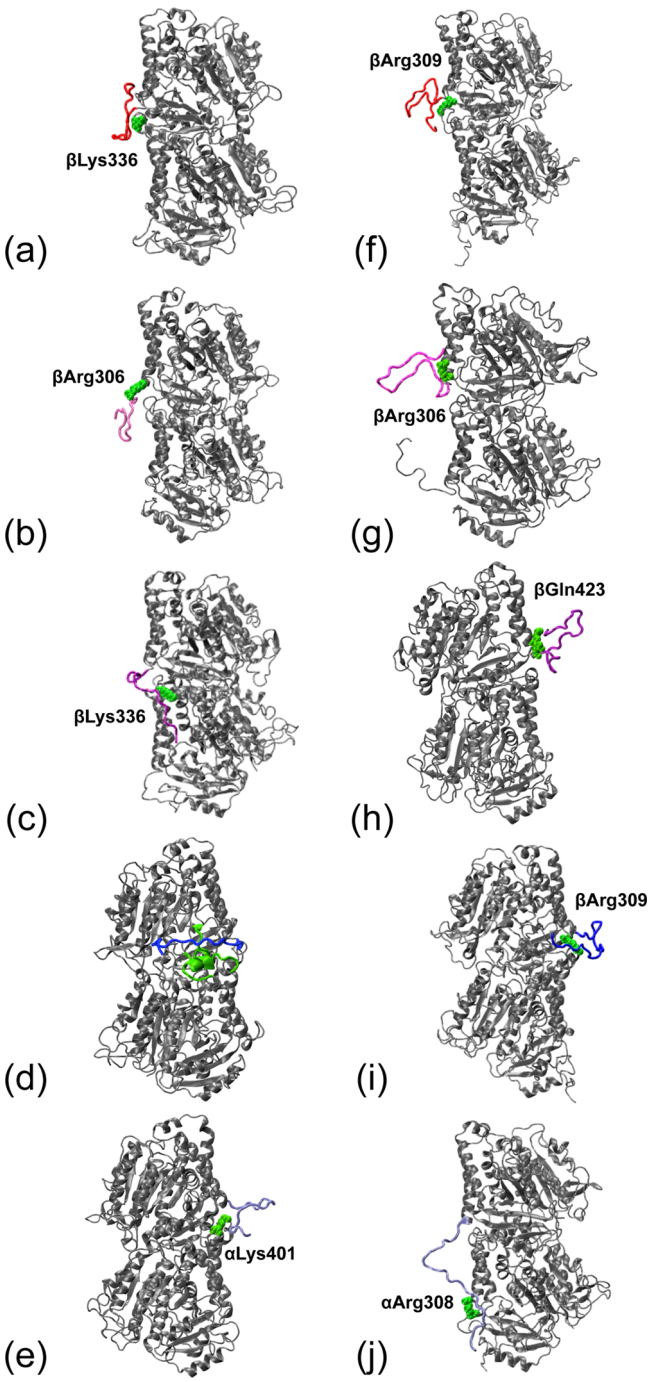

Figure 10. Snapshots from each of the MD simulations showing characteristic structures for the β-CTT bound to its anchor residue (from Figures SI-2 and SI-3) on the tubulin surface. The tubulin core is shown as a gray cartoon; the β-CTT is colored according to the trajectory number, and the anchor residue is shown as green van der Waals spheres. αI/βI isotype: anchor residues (a) βLys336, (b) βArg306, and (c) βLys336, (d) the complete NFL-TBS.40−63 peptide binding site[35] shown as a green cartoon, and (e) αLys401. αI/βIII isotype: anchor residues (f) βArg309, (g) βArg306, (h) βGln423, (i) βArg309, and (j) αArg308. Tubulin heterodimers are oriented as in Figure 4, except for panels a−c, f, g, and j, in which the protein has been rotated by 180° around the vertical axis to enhance the visibility. This figure was prepared using visual molecular dynamics.[48]

DISCUSSION

CTT Structure and Mobility. The MD study presented here significantly advances the time scales previously explored for complete tubulin systems. While sampling flexible tail conformations still presents a formidable challenge, the

DOI: 10.1021/acs.biochem.6b00988
Biochemistry XXXX, XXX, XXX−XXX

improved sampling we have obtained provides a more realistic view of their conformational dynamics. For both β-CTTs, we can directly compare the time average of each secondary structure over the five 100 ns MD simulations shown in Figure 6 with the results obtained by Luchko et al.[29] in their early work on the CTTs of nine human β-tubulin isotypes, which included the βI- and βIII-tails. In their study, the β-CTTs were modeled as independent systems, without taking into account the tubulin globular domain, and they performed MD and replica exchange MD simulations over the temperature range of 273−382 K. Figure 3 of ref 29 shows the resulting time average of each secondary structure over a 10 ns MD simulation at 311 K. While being mostly unstructured, the βI- and βIII-CTTs still showed a significant amount of transient helix, with residues being either α- or 3−10-helical at least 40% of the time. In our work, this was not seen; the interactions between the tubulin surface and the β-CTT may thus prevent the formation of helical secondary structures in the latter, favoring turn and coil conformations for the tail residues. Another point that has to be taken into account is the fact that the simulations performed by Luchko et al. used the AMBER99 force field, which has been shown to increase the helical content in unstructured peptides compared to the OPLS-AA force field used in our approach.[52] However, one should note that choosing the most appropriate force field for simulating folded tubulin core, the disordered terminal tails, and the interaction between these two parts of the protein is a delicate matter because, for example, Amber appears to be better suited for modeling electrostatic interactions between charged residues,[53] while OPLS seems to provide a better treatment of intrinsically disordered protein segments.[52]

While there are little experimental structural data available regarding tubulin CTTs, the radius of gyration distributions calculated from our MD simulations and shown in Figure 8 are compatible with estimates obtained by Asakawa et al.[54] from atomic force microscopy, which show the C-terminal domains as oval shapes on the tubulin surface with a size between 10 and 30 Å. We can also evaluate the radius of gyration for the CTTs by using Flory's equation,[55] $R_g = R_0 N^{\nu}$, where R_0 and ν are constant parameters and N is the number of residues in the peptidic chain. Values of R_0 and ν have been determined for intrinsically disordered proteins via SAXS experiments,[56,57] leading to an R_0 of 2.54 Å and a ν of 0.522, thus giving us radii of gyration of 11.5 and 13.3 Å for the βI-CTT and the βIII-CTT, respectively. These values concur remarkably well with those shown in Figure 8. If we compare the characteristic ratios of the CTTs, that is, the ratio of the average radius of gyration during a single trajectory to the radius of gyration predicted by Flory's law for a given isotype, we can see in Figure SI-8 how both isotypes present similar values, with the βIII-CTT being slightly more compact (i.e., presenting lower ratios) than its βI counterpart ($p = 0.07$).

One can note that any CTT conformation that might have been unique to a specific tubulin isoform would have been lost in experimental structural studies by data averaging because of the high isoform heterogeneity in tubulin samples. However, in a very recent work, Vemu et al.[58] managed to observe the structure of the isotypically pure human unmodified αI/βIII isotype by cryo-electron microscopy. Despite the chemical homogeneity of their sample, no density could be attributed to the CTTs, indicating that they are intrinsically disordered, which is in agreement with the high RMSDs and variety of structures that were observed during our five MS simulations of this isotype.

Tubulin Core−Tail Contacts. During all the MD trajectories performed in this study, the β-CTT formed contacts with a limited set of anchor residues located on the surface of the tubulin core, and these tail−body contacts are conserved throughout the rest of the simulation, although not necessarily with the same tail residues. As can be seen from the contact patterns shown in Figures 10, SI-2, and SI-3, the anchor residues for the αI/βI and αI/βIII isotypes are roughly the same and are located above the electronegative patch that partially covers the surface of the α-subunit (see Figure SI-6), near the interface between the α- and β-subunits. Some of these anchor residues, namely, αLys401 and βTrp344, were also highlighted as forming contacts with the β-CTT in a simulation work by Freedman et al.[30] on the αIV/βI isotype of human tubulin. Interestingly, this earlier study was conducted using MD calculations and simulated annealing and employed another force field, AMBER03, and an implicit solvent model (modified generalized Born[59]), while arriving at certain similar results, thus showing the robustness of molecular simulations for modeling this system. These results are also in agreement with those of a very recent NMR study by Wall et al.,[60] in which tubulin CTTs were isotopically labeled and their structure was investigated both as isolated peptides and within complete tubulin heterodimers (for the αI/βI isotype from *Tetrahymena thermophila*). In both cases, the CTTs are fully disordered, but they display significant chemical shift differences between the isolated peptides and tails in the context of the full dimer, thus indicating the CTTs interact with the ordered tubulin body. In addition, the CTTs show heterogeneity in association with the tubulin body, which concurs with the variety of anchor residues found in our work.

In our study, the core residues contacted by the βI-tails tended to be more clustered in the α/β-interface region than the for the βIII-CTT. We also observed individual cases in which each of the two isotypes displayed a specific binding pattern that was not observed for the other; this will of course require more extensive investigation. For example, in trajectory 5, the βIII-CTT adopted an extended conformation and bound anchor residues located on the lowest part of the tubulin α-subunit (Figure 10j). This binding mode of the β-CTT behind the electronegative groove covering the surface of the α-subunit (see Figure SI-8) is likely to be distinctive of the αI/βIII isotype, which is six residues longer than the βI-tail and, in addition to the numerous negatively charged glutamates commonly found in C-terminal tails, is terminated by a positively charged lysine residue. On the other hand, the αI/βI-tubulin isotype presented a specific binding mode in trajectory 4, where the βI-CTT extends to cover the preferential binding site for the NFL-TBS.40−63 peptide that was highlighted in our previous docking study[30] (see Figure 10d). Quite remarkably, this binding site coincides with a deep cleft within the electronegative patch covering the tubulin body surface (see Figure SI-8a). More generally, mapping the contact patterns from Figure 9 on the tubulin body's surface (see Figures SI-9 and SI-10) allows us to see how the βI-CTT contacts are more concentrated in the α/β-interface region that borders the putative binding site, while the βIII-CTT movements sweep out a more vertical pattern (and present a broader distribution of its θ angles, as seen in Figure SI-10c). This is of particular interest, because this peptide has been shown to specifically inhibit microtubule formation in glioma cells,[34] and the βIII-

DOI: 10.1021/acs.biochem.6b00988
Biochemistry XXXX, XXX, XXX−XXX

tubulin isotype is known to be overexpressed in several tumor types.[61] Therefore, our results allow us to formulate a first hypothesis for the NFL-TBS.40−63 peptide's specificity for glioma cells on a molecular level. The mobility patterns of the CTTS (shown in Figure SI-9) may suggest a higher affinity between the NFL-TBS.40−63 peptide and βIII-tubulin, compared to that for βI-tubulin, as the vertically distributed contacts may encroach less on the peptide's putative binding site. As glioma cells comprise a higher proportion of βIII-tubulin, they would thus be more affected by the NFL-TBS.40−63 peptide's antimitotic action than normal cells.

CONCLUDING REMARKS

Using a combination of modeling approaches, we investigated the mobility and binding modes on the tubulin surface of the β-C-terminal tails for the human αI/βI and αI/βIII isotypes. To the best of our knowledge, this is the first time that complete models (i.e., including the C-terminal tails) have been built for two human β-tubulin isotypes and jointly investigated using long time-scale (5 × 100 ns for each isotype) all-atom molecular dynamics simulations. While displaying similar contacts with residues located next to the α/β-interface, the isotypes differ in that the βI-tails may be more likely to form contacts in the interface and more particularly near the NFL-TBS.40−63 peptide binding site, thus potentially decreasing the affinity between βI-tubulin and this antimitotic compound and providing us with a first hypothesis regarding the peptide's enhanced activity in glioma cells (in which the βIII-tubulin isotype is known to be overexpressed). However, we cannot yet draw any final conclusions, as the differences in the contact and mobility patterns for both isotypes could also be due to insufficient sampling during our simulations. Additional work is needed to confirm our hypothesis. In particular, we plan to perform new molecular docking studies of the NFL-TBS.40−63 peptide on the αI/βI- and αI/βIII-tubulin isotypes that will include the tubulin C-terminal tails and take their flexibility into account. Another important issue is the fact that CTTs can be subject to numerous post-translational modifications, which impacts their structure and dynamics, and are also likely to have an effect on the recognition process between tubulin and its various ligands (such as other proteins, peptides, or smaller antimitotic compounds). One can also reflect on how embedding a tubulin heterodimer in a microtubule structure will impact CTT mobility. Bocquet et al.[33] showed that the NFL-TBS.40−63 peptide inhibits MT polymerization in vitro by binding unpolymerized tubulin, while having no effect on the stability of assembled MTs. CTTs protruding from a MT surface might present a specific mobility pattern, with an enhanced coverage of the NFL-TBS.40−63 peptide binding site, which would hinder the interaction between the peptide and the MT surface. Addressing this issue, however, will require costly calculations involving several interacting tubulin heterodimers.

More generally, our work opens up new perspectives for the understanding on a molecular level of the resistance to usual tubulin binding agents, such as paclitaxel, because it has been related to the overexpression of the βIII isotype.[22,29,62,63] In addition, our two structural models allow systematic drug binding studies of both isotypes, thus permitting the development of drugs that will preferentially target cancer cells, potentially reducing the side effects that are usually associated with chemotherapies.

ASSOCIATED CONTENT

Supporting Information

The Supporting Information is available free of charge on the ACS Publications website at DOI: 10.1021/acs.biochem.6b00988.

Additional data regarding the tubulin modeling, including sequence identities, Modeller scores, root-mean-square fluctuations on the β-CTTs, and detailed core−tail contact patterns (PDF)

Animated gifs of all 10 MD trajectories for both tubulin isotypes (ZIP)

AUTHOR INFORMATION

Corresponding Author

*E-mail: sacquin@ibpc.fr. Phone: +33 58 41 51 65.

ORCID

Sophie Sacquin-Mora: 0000-0002-2781-4333

Funding

Y.L. thanks the "Initiative d'Excellence" program from the French State (Grant "DYNAMO", ANR-11-LABX-011-01) for doctoral funding.

Notes

The authors declare no competing financial interest.

REFERENCES

(1) Aylett, C. H., Lowe, J., and Amos, L. A. (2011) New insights into the mechanisms of cytomotive actin and tubulin filaments. *Int. Rev. Cell Mol. Biol. 292*, 1−71.

(2) Luduena, R. F. (1998) Multiple forms of tubulin: different gene products and covalent modifications. *Int. Rev. Cytol. 178*, 207−275.

(3) Rezania, V., Azarenko, O., Jordan, M. A., Bolterauer, H., Luduena, R. F., Huzil, J. T., and Tuszynski, J. A. (2008) Microtubule assembly of isotypically purified tubulin and its mixtures. *Biophys. J. 95*, 1993−2008.

(4) Katsetos, C. D., Reginato, M. J., Baas, P. W., D'Agostino, L., Legido, A., Tuszyn Ski, J. A., Draberova, E., and Draber, P. (2015) Emerging microtubule targets in glioma therapy. *Seminars in pediatric neurology 22*, 49−72.

(5) Mariani, M., Karki, R., Spennato, M., Pandya, D., He, S., Andreoli, M., Fiedler, P., and Ferlini, C. (2015) Class III beta-tubulin in normal and cancer tissues. *Gene 563*, 109−114.

(6) Kavallaris, M. (2010) Microtubules and resistance to tubulin-binding agents. *Nat. Rev. Cancer 10*, 194−204.

(7) Serrano, L., de la Torre, J., Maccioni, R. B., and Avila, J. (1984) Involvement of the carboxyl-terminal domain of tubulin in the regulation of its assembly. *Proc. Natl. Acad. Sci. U. S. A. 81*, 5989−5993.

(8) Sackett, D. L., Bhattacharyya, B., and Wolff, J. (1985) Tubulin subunit carboxyl termini determine polymerization efficiency. *J. Biol. Chem. 260*, 43−45.

(9) Serrano, L., Wandosell, F., de la Torre, J., and Avila, J. (1988) Effect of specific proteolytic cleavages on tubulin polymer formation. *Biochem. J. 252*, 683−691.

(10) Wolff, J., Sackett, D. L., and Knipling, L. (1996) Cation selective promotion of tubulin polymerization by alkali metal chlorides. *Protein Sci. 5*, 2020−2028.

(11) Joe, P. A., Banerjee, A., and Luduena, R. F. (2009) Roles of beta-tubulin residues Ala428 and Thr429 in microtubule formation in vivo. *J. Biol. Chem. 284*, 4283−4291.

(12) Yadav, S., Verma, P. J., and Panda, D. (2014) C-terminal region of MAP7 domain containing protein 3 (MAP7D3) promotes microtubule polymerization by binding at the C-terminal tail of tubulin. *PLoS One 9*, e99539.

(13) Roll-Mecak, A. (2015) Intrinsically disordered tubulin tails: complex tuners of microtubule functions? *Semin. Cell Dev. Biol. 37*, 11−19.

DOI: 10.1021/acs.biochem.6b00988
Biochemistry XXXX, XXX, XXX−XXX

(14) Bailey, M. E., Sackett, D. L., and Ross, J. L. (2015) Katanin Severing and Binding Microtubules Are Inhibited by Tubulin Carboxy Tails. *Biophys. J. 109*, 2546−2561.
(15) Luduena, R. F. (2008) in *The Role of Microtubules in Cell Biology, Neurobiology, and Oncology* (Fojo, A. T., Ed.) pp 105−121, Humana Press, Totowa, NJ.
(16) Janke, C. (2014) The tubulin code: molecular components, readout mechanisms, and functions. *J. Cell Biol. 206*, 461−472.
(17) Sugiura, M., Maccioni, R. B., Cann, J. R., York, E. J., Stewart, J. M., and Kotovych, G. (1987) A proton magnetic resonance and a circular dichroism study of the solvent dependent conformation of the synthetic tubulin fragment Ac tubulin, alpha (430−441) amide and its interaction with substance-P. *J. Biomol. Struct. Dyn. 4*, 1105−1117.
(18) Otter, A., and Kotovych, G. (1988) The solution conformation of the synthetic tubulin fragment AC-tubulin-alpha(430−441)-amide based on two-dimensional ROESY experiments. *Can. J. Chem. 66*, 1814−1820.
(19) Amos, L. A. (2011) What tubulin drugs tell us about microtubule structure and dynamics. *Semin. Cell Dev. Biol. 22*, 916−926.
(20) Dostal, V., and Libusova, L. (2014) Microtubule drugs: action, selectivity, and resistance across the kingdoms of life. *Protoplasma 251*, 991−1005.
(21) Massarotti, A., Coluccia, A., Silvestri, R., Sorba, G., and Brancale, A. (2012) The tubulin colchicine domain: a molecular modeling perspective. *ChemMedChem 7*, 33−42.
(22) Freedman, H., Huzil, J. T., Luchko, T., Luduena, R. F., and Tuszynski, J. A. (2009) Identification and characterization of an intermediate taxol binding site within microtubule nanopores and a mechanism for tubulin isotype binding selectivity. *J. Chem. Inf. Model. 49*, 424−436.
(23) Rendine, S., Pieraccini, S., and Sironi, M. (2010) Vinblastine perturbation of tubulin protofilament structure: a computational insight. *Phys. Chem. Chem. Phys. 12*, 15530−15536.
(24) Chakraborti, S., Chakravarty, D., Gupta, S., Chatterji, B. P., Dhar, G., Poddar, A., Panda, D., Chakrabarti, P., Ghosh Dastidar, S., and Bhattacharyya, B. (2012) Discrimination of ligands with different flexibilities resulting from the plasticity of the binding site in tubulin. *Biochemistry 51*, 7138−7148.
(25) Mane, J. Y., Semenchenko, V., Perez-Pineiro, R., Winter, P., Wishart, D., and Tuszynski, J. A. (2013) Experimental and computational study of the interaction of novel colchicinoids with a recombinant human alphaI/betaI-tubulin heterodimer. *Chem. Biol. Drug Des. 82*, 60−70.
(26) Liao, S. Y., Mo, G. Q., Chen, J. C., and Zheng, K. C. (2014) Exploration of the binding mode between (−)-zampanolide and tubulin using docking and molecular dynamics simulation. *J. Mol. Model. 20*, 2070.
(27) Kumbhar, B. V., Borogaon, A., Panda, D., and Kunwar, A. (2016) Exploring the Origin of Differential Binding Affinities of Human Tubulin Isotypes alphabetaII, alphabetaIII and alphabetaIV for DAMA-Colchicine Using Homology Modelling, Molecular Docking and Molecular Dynamics Simulations. *PLoS One 11*, e0156048.
(28) Peng, L. X., Hsu, M. T., Bonomi, M., Agard, D. A., and Jacobson, M. P. (2014) The free energy profile of tubulin straight-bent conformational changes, with implications for microtubule assembly and drug discovery. *PLoS Comput. Biol. 10*, e1003464.
(29) Luchko, T., Torin Huzil, J., Stepanova, M., and Tuszynski, J. (2008) Conformational analysis of the carboxy-terminal tails of human beta-tubulin isotypes. *Biophys. J. 94*, 1971−1982.
(30) Freedman, H., Luchko, T., Luduena, R. F., and Tuszynski, J. A. (2011) Molecular dynamics modeling of tubulin C-terminal tail interactions with the microtubule surface. *Proteins: Struct., Funct., Genet. 79*, 2968−2982.
(31) Panneerselvam, M., Muthu, K., Jayaraman, M., Sridharan, U., Jenardhanan, P., and Ramadas, K. (2013) Molecular dynamic simulations of the tubulin-human gamma synuclein complex: structural insight into the regulatory mechanism involved in inducing resistance against Taxol. *Mol. BioSyst. 9*, 1470−1488.
(32) Chakraborty, S., and Zheng, W. (2015) Decrypting the structural, dynamic, and energetic basis of a monomeric kinesin interacting with a tubulin dimer in three ATPase states by all-atom molecular dynamics simulation. *Biochemistry 54*, 859−869.
(33) Bocquet, A., Berges, R., Frank, R., Robert, P., Peterson, A. C., and Eyer, J. (2009) Neurofilaments bind tubulin and modulate its polymerization. *J. Neurosci. 29*, 11043−11054.
(34) Berges, R., Balzeau, J., Peterson, A. C., and Eyer, J. (2012) A tubulin binding peptide targets glioma cells disrupting their microtubules, blocking migration, and inducing apoptosis. *Mol. Ther. 20*, 1367−1377.
(35) Laurin, Y., Savarin, P., Robert, C. H., Takahashi, M., Eyer, J., Prevost, C., and Sacquin-Mora, S. (2015) Investigating the Structural Variability and Binding Modes of the Glioma Targeting NFL-TBS.40−63 Peptide on Tubulin. *Biochemistry 54*, 3660−3669.
(36) Chen, K., Huzil, J. T., Freedman, H., Ramachandran, P., Antoniou, A., Tuszynski, J. A., and Kurgan, L. (2008) Identification of tubulin drug binding sites and prediction of relative differences in binding affinities to tubulin isotypes using digital signal processing. *J. Mol. Graphics Modell. 27*, 497−505.
(37) Fiser, A., Do, R. K., and Sali, A. (2000) Modeling of loops in protein structures. *Protein Sci. 9*, 1753−1773.
(38) Fiser, A., and Sali, A. (2003) Modeller: generation and refinement of homology-based protein structure models. *Methods Enzymol. 374*, 461−491.
(39) UniProt Consortium (2015) UniProt: A hub for protein information. *Nucleic Acids Res. 43*, D204−D212.
(40) Krivov, G. G., Shapovalov, M. V., and Dunbrack, R. L., Jr. (2009) Improved prediction of protein side-chain conformations with SCWRL4. *Proteins: Struct., Funct., Genet. 77*, 778−795.
(41) Pronk, S., Pall, S., Schulz, R., Larsson, P., Bjelkmar, P., Apostolov, R., Shirts, M. R., Smith, J. C., Kasson, P. M., van der Spoel, D., Hess, B., and Lindahl, E. (2013) GROMACS 4.5: a high-throughput and highly parallel open source molecular simulation toolkit. *Bioinformatics 29*, 845−854.
(42) Kaminski, G. A., Friesner, R. A., Tirado-Rives, J., and Jorgensen, W. L. (2001) Evaluation and reparametrization of the OPLS-AA force field for proteins via comparison with accurate quantum chemical calculations on peptides. *J. Phys. Chem. B 105*, 6474−6487.
(43) Jorgensen, W. L., Chandrasekhar, J., Madura, J. D., Impey, R. W., and Klein, M. L. (1983) Comparison of Simple Potential Functions for Simulating Liquid Water. *J. Chem. Phys. 79*, 926−935.
(44) Bussi, G., Donadio, D., and Parrinello, M. (2007) Canonical sampling through velocity rescaling. *J. Chem. Phys. 126*, 014101.
(45) Hess, B., Bekker, H., Berendsen, H. J. C., and Fraaije, J. (1997) LINCS: A linear constraint solver for molecular simulations. *J. Comput. Chem. 18*, 1463−1472.
(46) Essmann, U., Perera, L., Berkowitz, M. L., Darden, T., Lee, H., and Pedersen, L. G. (1995) A SMOOTH PARTICLE MESH EWALD METHOD. *J. Chem. Phys. 103*, 8577−8593.
(47) Parrinello, M., and Rahman, A. (1981) Polymorphic transitions in single crystals: A new molecular dynamics method. *J. Appl. Phys. 52*, 7182−7190.
(48) Humphrey, W., Dalke, A., and Schulten, K. (1996) VMD: visual molecular dynamics. *J. Mol. Graphics 14*, 27−38.
(49) Baker, N. A., Sept, D., Joseph, S., Holst, M. J., and McCammon, J. A. (2001) Electrostatics of nanosystems: application to microtubules and the ribosome. *Proc. Natl. Acad. Sci. U. S. A. 98*, 10037−10041.
(50) Frishman, D., and Argos, P. (1995) Knowledge-based protein secondary structure assignment. *Proteins: Struct., Funct., Genet. 23*, 566−579.
(51) Janin, J. (2005) Assessing predictions of protein-protein interaction: the CAPRI experiment. *Protein Sci. 14*, 278−283.
(52) Smith, M. D., Rao, J. S., Segelken, E., and Cruz, L. (2015) Force-Field Induced Bias in the Structure of Abeta21−30: A Comparison of OPLS, AMBER, CHARMM, and GROMOS Force Fields. *J. Chem. Inf. Model. 55*, 2587−2595.

DOI: 10.1021/acs.biochem.6b00988
Biochemistry XXXX, XXX, XXX−XXX

(53) Debiec, K. T., Gronenborn, A. M., and Chong, L. T. (2014) Evaluating the strength of salt bridges: a comparison of current biomolecular force fields. *J. Phys. Chem. B 118*, 6561−6569.
(54) Asakawa, H., Ikegami, K., Setou, M., Watanabe, N., Tsukada, M., and Fukuma, T. (2011) Submolecular-scale imaging of alpha-helices and C-terminal domains of tubulins by frequency modulation atomic force microscopy in liquid. *Biophys. J. 101*, 1270−1276.
(55) Flory, P. J. (1969) *Statistical mechanics of chain molecules*, Interscience-Wiley Publishers, New York.
(56) Bernado, P., and Svergun, D. I. (2012) Structural analysis of intrinsically disordered proteins by small-angle X-ray scattering. *Mol. BioSyst. 8*, 151−167.
(57) Kikhney, A. G., and Svergun, D. I. (2015) A practical guide to small angle X-ray scattering (SAXS) of flexible and intrinsically disordered proteins. *FEBS Lett. 589*, 2570−2577.
(58) Vemu, A., Atherton, J., Spector, J. O., Szyk, A., Moores, C. A., and Roll-Mecak, A. (2016) Structure and Dynamics of Single-isoform Recombinant Neuronal Human Tubulin. *J. Biol. Chem. 291*, 12907−12915.
(59) Onufriev, A., Bashford, D., and Case, D. A. (2004) Exploring protein native states and large-scale conformational changes with a modified generalized born model. *Proteins: Struct., Funct., Genet. 55*, 383−394.
(60) Wall, K. P., Pagratis, M., Armstrong, G., Balsbaugh, J. L., Verbeke, E., Pearson, C. G., and Hough, L. E. (2016) Molecular Determinants of Tubulin's C-Terminal Tail Conformational Ensemble. *ACS Chem. Biol. 11*, 2981−2990.
(61) Katsetos, C. D., Draberova, E., Legido, A., Dumontet, C., and Draber, P. (2009) Tubulin targets in the pathobiology and therapy of glioblastoma multiforme. I. Class III beta-tubulin. *J. Cell. Physiol. 221*, 505−513.
(62) Goncalves, A., Braguer, D., Kamath, K., Martello, L., Briand, C., Horwitz, S., Wilson, L., and Jordan, M. A. (2001) Resistance to Taxol in lung cancer cells associated with increased microtubule dynamics. *Proc. Natl. Acad. Sci. U. S. A. 98*, 11737−11742.
(63) Kamath, K., Wilson, L., Cabral, F., and Jordan, M. A. (2005) BetaIII-tubulin induces paclitaxel resistance in association with reduced effects on microtubule dynamic instability. *J. Biol. Chem. 280*, 12902−12907.
(64) *The PyMOL Molecular Graphics System*, version 1.3r1 (2010) Schrodinger, LLC, Portland, OR.

DOI: 10.1021/acs.biochem.6b00988
Biochemistry XXXX, XXX, XXX−XXX